A Compact Triaxial Hall Sensor Compatible with Standard CMOS Process Leveraging Horizontal and Vertical Current Flow within Deep N-Well

Yuhao Wang, Toshihisa Tanaka, Tomochika Harada, *Member, IEEE*, Masanori Hashimoto, *Senior Member, IEEE,* Ryo Shirai, *Member, IEEE*

***Abstract*— This paper presents a CMOS-compatible triaxial Hall sensor featuring a novel vertical Hall device (VHD) structure that achieves high sensitivity and low cross-axis interference. The proposed sensor utilizes both vertical and horizontal Hall effects by exploiting the high conductivity of the Deep N-Well (DNW) layer, thereby eliminating the need for space-consuming shallow trench isolation (STI). The architecture supports compact and highly sensitive sensor integration by avoiding exclusive reliance on the vertical Hall effect, which is highly dependent on device dimensions. Moreover, a spatially symmetrical emitter structure is introduced to effectively minimize cross sensitivity. The sensor was fabricated using a standard 180 nm TSMC CMOS process and experimentally evaluated using on-chip operational amplifiers, whose bias conditions were adjusted to maximize the voltage gain during measurement. The measured sensitivities were 967.5 mV/T for the vertical Hall element and 656.7 mV/T for the horizontal Hall element. Angular response measurements confirm cross sensitivities below 0.01 %, demonstrating excellent directional selectivity and validating the effectiveness of the proposed structure.**

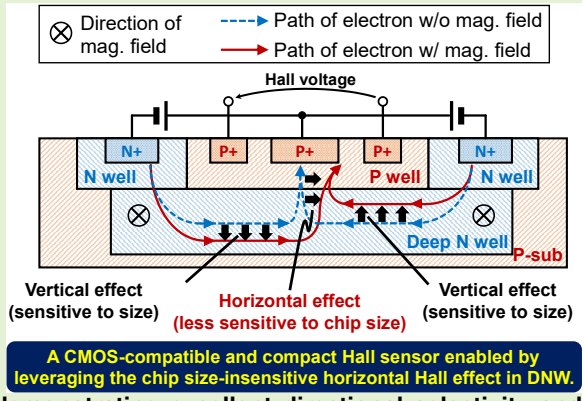

***Index Terms*— Triaxial magnetic sensor, Hall sensor, complementary metal–oxide–semiconductor (CMOS) process.**

I. Introduction

HALL sensors are employed in numerous domains–such as robotics, automotive applications [1]–[4], positioning systems [5], current measurement [6], [7], and medical instrumentation [8], [9]. To satisfy diverse application requirements, various magnetic-sensing technologies have been explored, including giant magnetoresistive (GMR) sensors [10], fluxgate sensors [11], anisotropic magnetoresistance (AMR) sensors [12], tunneling magnetoresistance (TMR) sensors [13], and microelectromechanical systems (MEMS)-based magnetic sensors. Although the intrinsic sensitivity of Hall-effect sensors is lower than that of certain magnetoresistive or MEMS-based devices [14], [15], Hall sensors remain a dominant technology in the commercial magnetic sensor market. This is largely due to their compatibility with CMOS processes, compact footprint, low cost, and sufficient sensitivity for many high-volume applications. Indeed, Hall and magnetoresistive sensors together account for approximately 98 % of the magnetic sensor market share [16].

Conventional planar Hall sensors are inherently limited to detecting magnetic fields perpendicular to the chip surface, which restricts their applicability in scenarios requiring triaxial sensing. To address this, three principal structural approaches have been developed. The first uses three orthogonally arranged horizontal Hall devices (HHDs), each sensitive to a single axis; however, this method often necessitates multiple dies and precise alignment, complicating packaging [17], [18]. The second approach integrates ferromagnetic concentrators above planar sensors to redirect magnetic fields toward the sensitive axis, enabling full-axis detection [19]–[21]. Nevertheless, this requires non-standard post-processing, which increases fabrication cost and complexity. The third relies on vertical Hall devices (VHDs) fabricated via standard CMOS processes, which can detect in-plane magnetic fields without additional structures. However, due to their current flow geometry and electrode configuration, conventional VHDs have limited sensitivity to out-of-plane (Z-axis) magnetic fields [22]–[26]. As a result, additional structures or complementary sensing elements are typically required to enable Z-axis magnetic field detection in triaxial sensor implementations. In some designs, VHDs and HHDs are combined to leverage their respective

This work was supported by JSPS KAKENHI Grant Numbers JP22K17867 and 25K21172. (Yuhao Wang and Toshihisa Tanaka are co-first authors.) (Corresponding author: Ryo Shirai)

Yuhao Wang, Toshihisa Tanaka, Masanori Hashimoto, and Ryo Shirai are with the Department of Informatics, Kyoto University, Kyoto 606-8501, Japan (e-mail: {wang.yuhao.83p, tanaka.toshihisa.52z}@st.kyoto-u.ac.jp; {hashimoto, shirai}@i.kyoto-u.ac.jp). Tomochika Harada is with the Department of Informatics and Electronics, Yamagata University, Yamagata 992-0038, Japan (e-mail: tharada@yz.yamagata-u.ac.jp).

directional sensitivities. On the other hand, this approach often faces challenges due to mismatched sensitivities and increased offset in the vertical devices [27]–[29], motivating further improvement in VHD performance.

To address the limitations of conventional multi-axis Hall sensor designs, this work proposes a compact, CMOS-compatible triaxial Hall sensor. The key idea lies in directing vertical current flow through the Deep N-Well (DNW) and P-Well regions, thereby enhancing the lateral deflection of carriers under in-plane magnetic fields. This mechanism amplifies the horizontal Hall effect and enables stronger signal generation within a limited volume. Unlike prior approaches based on shallow trench isolation (STI), the proposed design achieves current steering through conductivity differences among CMOS layers. This eliminates the need for STI structures and supports compact integration, thereby increasing the Hall voltage output per unit area. The sensor is fabricated using a TSMC 180 nm standard CMOS process, with no additional post-processing required.

The rest of this paper is organized as follows. Section II reviews prior work on CMOS-based magnetic sensors. Section III introduces the proposed sensor architecture and explains the operating principles in detail. Section IV presents experimental results obtained from fabricated chips, along with performance analysis and discussion. Finally, Section V concludes the paper.

II. Related Work

Triaxial Hall sensors based on standard CMOS processes have been explored through three principal architectural approaches. This section reviews each of these methods, focusing on their operational principles, advantages, and inherent limitations.

A. Triple Horizontal Hall Device Configuration

One common approach employs three horizontal Hall devices (HHDs) arranged orthogonally. Each device is inherently sensitive to magnetic fields perpendicular to the chip surface, enabling detection of X-, Y-, and Z-axis components [17], [18]. This configuration benefits from the maturity and high sensitivity of planar Hall structures. Fig.1 illustrates the structure and operation of an HHD on a p-type substrate, showing a top view of the layout. Although n-type wells are more commonly used in Hall elements due to higher electron mobility, a p-type representation is employed here for consistency with the p-type device implemented in our proposed structure described later in Section III. When a supply voltage is applied such that current flows from terminal B to D, holes move accordingly. In the absence of a magnetic field, carriers follow a straight path through the center. When a perpendicular magnetic field is applied, the Lorentz force bends the hole trajectory, as shown in Fig.1. This deflection causes a potential difference between terminals A and C, approximately proportional to the magnetic field strength. Thus, the vertical component of the magnetic field can be measured by detecting the Hall voltage between terminals A and C.

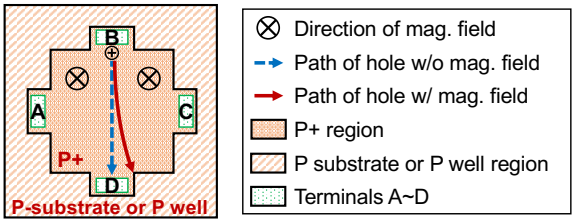

Fig. 1. Top view and operating principle of HHD.

However, achieving accurate triaxial measurement requires precise spatial alignment among the sensors. Implementation often involves multiple dies or stacked layers, which increases packaging complexity and manufacturing cost.

B. Planar Hall Devices with Magnetic Concentrators

Another method enhances the functionality of planar Hall devices by incorporating integrated magnetic concentrators (IMCs) [19], [21], [30]–[32]. A ferromagnetic layer placed above the Hall element redirects in-plane magnetic fields toward the Z direction, enabling full-vector magnetic field detection using a single planar device. This structure achieves high sensitivity, with reported values of 45 V/T for the Z axis and 22.5 V/T for the X and Y axes [19]. Despite its effectiveness, this technique requires non-standard post-processing steps, including multi-layer ferromagnetic deposition and precise alignment of the magnetic concentrator to the sensor chip [31]. Misalignment between the IMC and the Hall element can significantly degrade directional sensitivity [31]. Additionally, the implementation of magnetic concentrators often involves complex machining and assembly processes using ferromagnetic materials and bonding technologies, which complicate large-scale production [32].

C. Cross-Placed VHD Configuration

VHD [33] is a representative structure for sensing magnetic fields parallel to the chip surface. Unlike magnetic concentrator-based designs, VHDs can be fabricated entirely within standard CMOS processes, requiring no post-processing. Compatibility with baseline manufacturing flows enables cost-effective production and facilitates large-scale integration. As shown in Fig.2, the VHD comprises five terminals arranged in a metal layer. In the structure shown in Fig.2, STI structures are inserted between terminals to inhibit lateral current flow near the surface. Consequently, electrons injected from the outermost left and right N+ emitter terminals are diverted into the substrate and proceed laterally toward the central P+ collector. When a magnetic field is applied perpendicular to the current flow, typically along the X or Y axis depending on orientation, the Lorentz force induces an asymmetric vertical current distribution, as illustrated in Fig.2. This imbalance generates a lateral potential difference between two N+ sensing contacts on both sides of the P+ area, known as the Hall voltage. Here, it should be noted that while the use of STI is a common approach for controlling current flow in VHD implementations, alternative methods employing

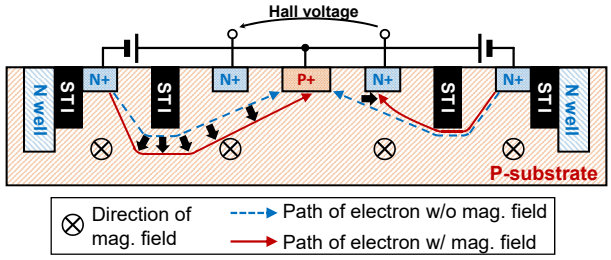

Fig. 2. Structure and operating principle of a typical CMOS VHD implementation employing STI to suppress surface shunting and steer the current path.

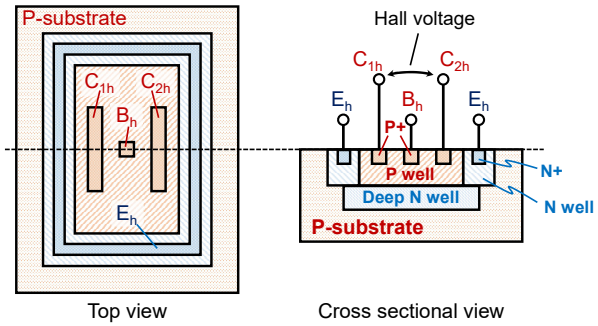

Fig. 3. Structure of the proposed vertical Hall sensor.

other conductive layers or structural designs have also been reported [24].

For triaxial sensing, two VHDs are often arranged orthogonally in a cross configuration. This arrangement enables detection of not only X- and Y-axis components but also Z-axis components using identical structures [22], [25]. However, the sensitivity to the Z-axis component remains approximately 10 % lower than that of the X and Y axes, primarily due to weaker deflection effects [22].

To achieve high sensitivity across all axes, some designs incorporate both vertical (VHD) and horizontal (HHD) Hall devices. In such hybrid configurations, VHDs are employed for in-plane field detection, whereas HHDs address the out-of-plane component [27]–[29]. Although this combination improves directional coverage, it introduces considerable calibration challenges. Sensitivity mismatches and offset variations between VHDs and HHDs frequently arise from structural and process-induced asymmetries.

Therefore, achieving consistent triaxial performance requires further improvements in VHD design. A primary limitation of conventional VHDs is the use of STI structures, which pose notable drawbacks: they occupy substantial die area and increase cross-sensitivity, leading to erroneous readings under magnetic fields not aligned with the target sensing direction. Eliminating these space-consuming STI structures is thus an important step toward realizing compact, accurate, and fully CMOS-compatible sensors.

III. Proposed Method

To achieve CMOS-compatible sensor integration without requiring STI structure, which limits the miniaturization of sensor volume and negatively affects cross-sensitivity, this section proposes a triaxial Hall sensor architecture with high sensitivity and low cross-sensitivity. Section III-A proposes a VHD structure without STI, which is designed to detect magnetic fields parallel to the chip surface (X- and Y-axis), and describes its operating principle in detail. Section III-B presents the HHD structure, which is implemented using a conventional layout, to sense magnetic fields perpendicular to the chip surface (Z-axis), and briefly discusses its operation.

A. Vertical Sensor Structure and Principle

Fig. 3 illustrates the structure of the proposed VHD. The sensor utilizes a five-contact vertical Hall device configuration, where a DNW layer is embedded beneath the N-Well. This structure allows the current to flow not only horizontally but also vertically along the die surface, reminiscent of conventional methods that utilize a conductive buried layer to control the current distribution [24]. Each sensor consists of an emitter ring (E_h) positioned at the edges, a central base (B_h), and two collectors (C_{1h} and C_{2h}) located on either side of the base. In Fig. 3, which represents the sensor designed to detect magnetic fields along the up–down direction on the paper (in-plane B_y field), the emitter ring is intentionally designed in a rectangular rather than circular shape. This geometry enhances the lateral current component flowing horizontally across the paper, which effectively contributes to Hall voltage generation, while reducing the vertically directed in-plane currents that do not contribute to the Hall signal and merely increase power consumption. X and Y sensors have an identical layout but are placed perpendicularly on the chip to detect magnetic fields in the X and Y directions, respectively.

Fig. 4 presents the operating principle of the proposed VHD. The proposed VHD structure is designed to leverage two types of Hall effects: the horizontal effect and the vertical effect. Here, *horizontal* and *vertical* refer to the direction of carrier deflection induced by the Lorentz force, not the direction of the electrical current.

The horizontal effect describes how charge carriers experience the Lorentz force and move in the horizontal direction. Applying voltage across the emitter ring (E_{1x}) and the base (B_{1x}) initiates a current flow from these regions. In this configuration, the current preferentially flows through the DNW rather than the P-Well, primarily due to the higher electrical conductivity of the DNW compared to the P-Well, as will be quantitatively discussed in a successive section. This conductivity contrast enables the DNW to guide a larger portion of the current vertically, as illustrated in Fig. 4. When an external magnetic field in the horizontal direction is applied, the electrons are subject to the Lorentz force and their trajectories bend. In the horizontal direction, the current path is deflected toward either the left or right collector, depending on the field polarity, resulting in a potential difference between the two collectors, which is appeared as the Hall voltage.

The vertical effect adopts the same principle as the traditional VHD structure, where the Lorentz force deflects charge carriers vertically in the chip. Specifically in Fig. 4, electrons emitted from the left emitter are bent downward, while those

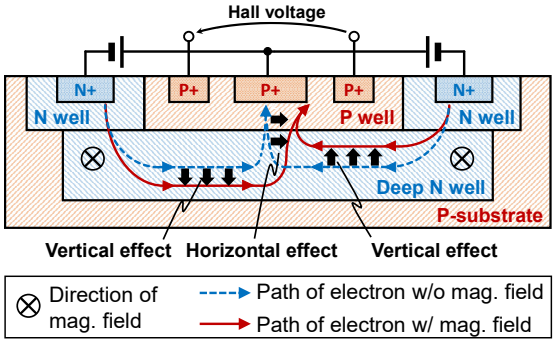

Fig. 4. Illustration of the horizontal and vertical Hall effects occurring within the proposed VHD structure.

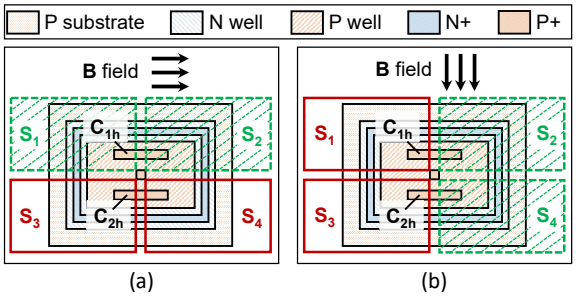

Fig. 5. Potential distribution in each region of the X-axis sensor under X- and Y-directed magnetic fields.

from the right emitter are deflected upward. This movement creates an asymmetry in the carrier distribution, which enhances the potential difference between the two collectors on the chip, resulting in a stronger Hall voltage output.

The proposed design utilizes a DNW region with significantly higher conductivity, which plays a critical role in guiding the current flow such that both vertical and horizontal Hall effects can be exploited for high sensitivity. The high conductivity of the DNW layer effectively attracts more current into deeper regions of the substrate than STI-based structures. This deeper current distribution brings two main advantages: first, it allows the Lorentz force to act more efficiently over a longer carrier path, thereby increasing the resulting Hall voltage; second, it enables the sensor structure to operate without the need for shallow confinement structures such as STI layers. Consequently, the absence of STI permits a more compact sensor design with reduced horizontal dimension area, while maintaining high sensitivity and robust performance.

In practical applications, external magnetic fields do not necessarily align with the principal coordinate axes. Each axis-specific sensor must therefore respond exclusively to the magnetic field component along its designated direction, while remaining insensitive to orthogonal components. For instance, an X-axis sensor should produce an output corresponding only to the B_x component, and exhibit negligible response under B_y or B_z excitation.

To ensure directional selectivity and minimize cross-axis interference, the proposed design adopts an emitter ring structure promoting spatial separation and symmetry. Fig. 5 illustrates the sensing behavior of an X-axis sensor. The structure is symmetrically divided into four regions (S_1 to S_4). When

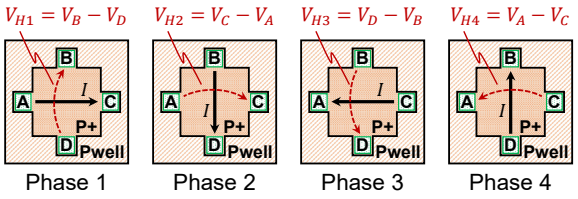

Fig. 6. Structure of HHD and measurement procedures of the current spinning method for offset cancellation.

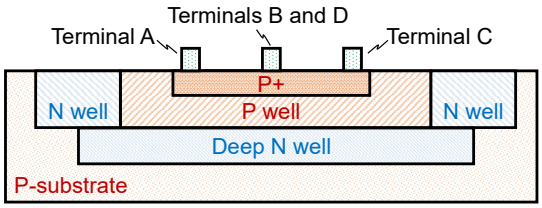

Fig. 7. Cross-sectional view of implemented HHD.

a magnetic field is applied along the X-axis, as shown in Fig.5(a), electrons in S_1 and S_2 (green shaded areas) travel through deeper DNW regions due to the vertical Hall effect, while those in S_3 and S_4 (red outlined areas) pass through shallower ones. Simultaneously, the horizontal Hall effect drives carriers downward, creating lower potentials in S_3 and S_4 than in S_1 and S_2. This potential gradient appears as a measurable Hall voltage between collectors C_{1h} and C_{2h}.

In contrast, when a magnetic field is applied along the Y-axis as shown in Fig. 5(b), vertical and horizontal effects occur symmetrically across S_1 to S_4. Although local potential differences arise within each subregion (S_1–S_4), the collectors C_{1h} and C_{2h} are each formed as single conductive regions spanning across two subregions (S_1 and S_2, and S_3 and S_4, respectively). The internal electrical connection within each collector ensures that these local potential variations are effectively averaged out within C_{1h} and C_{2h}, respectively. As a result, no net Hall voltage appears between the two collectors, confirming that the proposed VHD is insensitive to magnetic fields along the Y-axis.

B. Horizontal Sensor structure and Principle

Fig. 6 shows the structure of the HHD used in this study to sense magnetic fields along the Z axis, and its cross-sectional view is provided in Fig. 7. A p-type HHD configuration was adopted, which is structurally equivalent to conventional n-type Hall devices but implemented within a deep n-well (DNW) region for electrical isolation. The primary objective of this work is to demonstrate a low-cross-sensitivity, low-noise tri-axial sensing concept rather than to maximize sensitivity. Therefore, the p-type implementation was selected for its design simplicity and robust device isolation from other sensors and circuits, even though the carrier mobility of p-type material is lower than that of n-type. As shown in Fig. 1, the HHD consists of four terminals labeled A through D. Among them, a pair of opposing terminals is used for current injection, while the remaining pair is used to measure the Hall voltage. A major challenge in measuring the Hall voltage with HHDs is the presence of offset voltage components in

the output. In this work, offset cancellation is achieved using the current spinning method [6], [21], [34]–[36]. Using Fig. 6, we describe the industry-standard four-phase current-spinning procedure for offset cancellation. In Phase 1, current is applied from terminal A to C, and the Hall voltage between terminals B and D is measured as $V_{H1} = V_B - V_D$. In Phase 2, the current is rotated by $90°$: current flows from B to D, and the voltage between C and A is measured as $V_{H2} = V_C - V_A$. In Phases 3 and 4, the current direction is further rotated by $90°$ at each step ($C \rightarrow A$ and $D \rightarrow B$, respectively), and $V_{H3} = V_D - V_B$ and $V_{H4} = V_A - V_C$ are measured. Each of these four voltages contains both the true Hall component and a corresponding offset. However, by averaging the four measurements, the offset terms cancel due to the symmetry of the configuration [35], yielding

$$V_{\text{Hall}} = \frac{1}{4}\left(V_{H1} + V_{H2} + V_{H3} + V_{H4}\right). \tag{1}$$

IV. Evaluation

This section presents the performance evaluation of the proposed triaxial Hall sensor, which was fabricated using the TSMC 180 nm standard CMOS process. The evaluation consists of both simulation-based and hardware-based analyses.

A. Simulation-based evaluation of layer conductivities

This section validates the current path described in Section III-A by estimating the conductivity of each semiconductor layer using TCAD simulation. The current distribution in the proposed VHD is strongly influenced by the conductivity differences among the underlying layers. According to semiconductor band theory [37], the conductivity σ of an extrinsic semiconductor layer can be expressed as:

$$\sigma = nq\mu, \tag{2}$$

where n is the carrier concentration (cm^{-3}), q is the elementary charge (1.602×10^{-19} C), and μ is the carrier mobility ($\text{cm}^2/\text{V}\cdot\text{s}$). We extract carrier concentrations n and mobility μ with 3D TCAD simulations based on assumptions provided in [37] since detailed doping profiles are considered proprietary by the foundry and were not disclosed. Based on [37], for the DNW, the electron concentration is $n_e = 4.73 \times 10^{16}$ $[\text{cm}^{-3}]$, and the mobility is $\mu_e = 900$ $[\text{cm}^2/\text{V}\cdot\text{s}]$. For the P-Well, the hole concentration is $n_h = 3.05\times10^{16}$ $[\text{cm}^{-3}]$, and the mobility is $\mu_h = 300$ $[\text{cm}^2/\text{V}\cdot\text{s}]$. By substituting these values into Eq. (2), conductivities are calculated as follows: $\sigma_{\text{DNW}} = 6.81$ $[\text{S/cm}]$, $\sigma_{\text{PWell}} = 1.47$ $[\text{S/cm}]$. These results confirm that DNW, with its higher doping concentration and electron mobility, exhibits significantly greater conductivity than the P-Well, contributing to current transport and sensor performance, supporting the explanation in Section III-A about the operation principles of the proposed sensor.

B. Hardware evaluation setup

This section introduces the experimental setup used for hardware evaluation. Fig. 8 shows a photograph of the fabricated chip implementing the proposed Hall sensors using the TSMC 180 nm standard CMOS process. As shown in Fig. 8, the Hall sensor structures are fully covered by a dense dummy-metal shielding pattern. This shielding is intentionally implemented because the active regions of the proposed Hall devices are based on p-type wells, where incident light can generate photo-induced carriers in the PN junctions and consequently introduce additional offset and measurement errors. For this reason, optical inspection of the underlying Hall elements is not possible from the fabricated chip photograph alone. To clearly present the device geometry, Fig. 9 provides the corresponding layout view, which faithfully reflects the structural design of the Hall elements proposed in this work. The VHD occupies 400 µm×600 µm, with a base region of 50 µm×50 µm and a collector region of 47 µm×175 µm. The separation between base and collectors is 20 µm. The HHD occupies 30 µm×30 µm. Sensor outputs are connected to on-chip operational amplifiers to increase measurable voltage. The chip is wire-bonded directly to a printed circuit board (PCB) for measurement. To prevent measurement noise caused by ambient light exposure, all sensor regions are shielded by the top metal layer, as shown in Fig. 8.

Fig. 10 illustrates the experimental setup, and Fig. 11 presents a photograph of the actual measurement environment. The sensor-mounted PCB is placed between two coils with iron cores, which are driven by external current sources to generate a magnetic field. The PCB is fixed to a rotatable jig that enables precise orientation of the sensor. A Gauss meter is set to obtain a reference value of the magnetic field flux. By adjusting the current supplied to the coils, the applied magnetic field strength is controlled, and the sensor output voltage is recorded accordingly.

The amplifier used in this experiment is configured as an open-loop operational amplifier without a feedback network, in order to maximize the voltage gain. The bias voltage of the on-chip operational amplifiers was then carefully tuned to maximize the output amplitude of the Hall device while maintaining stable operation. According to circuit simulations, the amplifier exhibited a voltage gain of approximately 100× (40 dB) under optimal input range and bias conditions. However, in the actual measurements, the effective gain did not reach this ideal value because the output voltage range of the Hall device was not fully within the optimal input range of the amplifier. As a result, the voltage amplification was estimated to be in the range of approximately 10–30×, depending on the bias current and input voltage conditions. This bias adjustment ensured stable operation of the amplifier while maintaining sufficient dynamic range for the measured Hall voltages.

C. Evaluation of the proposed vertical Hall sensor

The performance of the proposed VHD, configurable to detect magnetic fields along the X or Y axis, was experimentally evaluated. A supply voltage of 1.6 V was applied between emitter and base terminals, yielding a drive current of 24 mA. By varying the current supplied to the coils in Fig. 11, the magnetic flux density in the X direction at the sensor position was swept from −77.2 mT to 77.3 mT. The results are shown in Fig. 12. When the magnetic flux density around the device

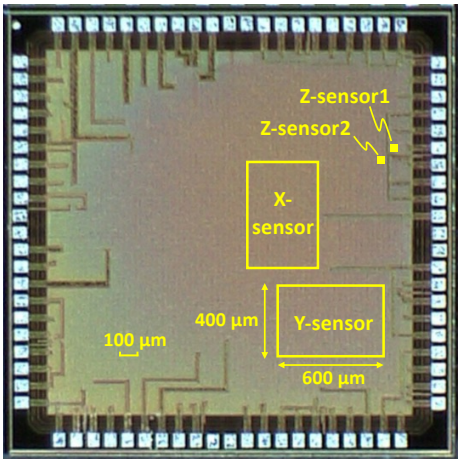

Fig. 8. Photo of chip fabricated using TSMC 180 nm CMOS process.

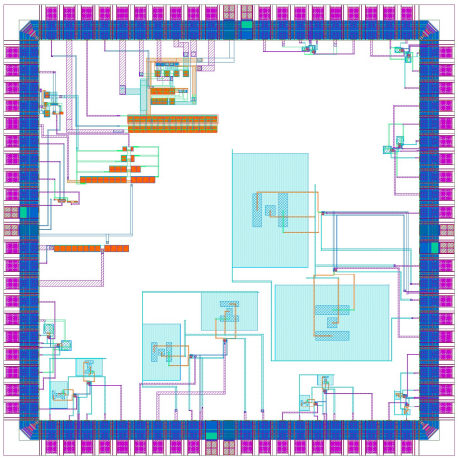

Fig. 9. Layout view of fabricated chip.

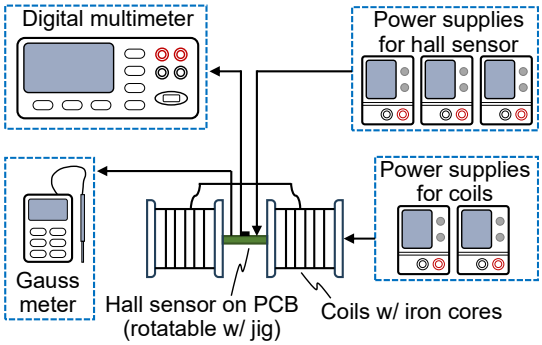

Fig. 10. Schematic of experimental setup.

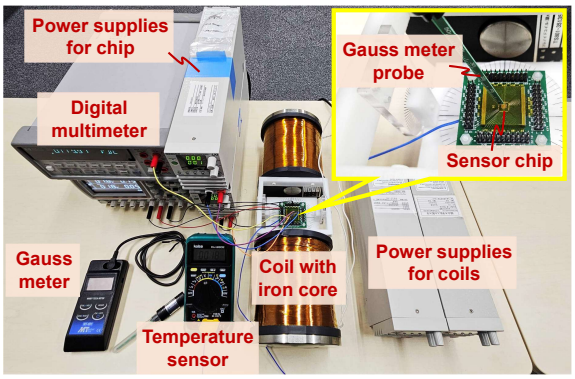

Fig. 11. Photo of evaluation environment.

was $B_x = 0$, the output voltage of the proposed sensor, as observed using a digital multimeter (KAISE KU-2602), varied within a range of approximately -1 mV to $+1$ mV. This behavior indicates that the output voltage was centered near zero while exhibiting random fluctuations attributed to noise. While the residual DC offset could not be directly characterized with the present measurement setup, an indicative offset value can be discussed based on the linear regression result, as described below. As shown in Fig. 12, the output voltage of the proposed VHD exhibits a highly linear response to the applied magnetic field, with a coefficient of determination $R^2 = 0.9973$. The measured sensitivity was 967.5 mV/T. Although the output voltage at zero magnetic field could not be directly measured with sufficient accuracy, an indicative offset value can be estimated from the linear regression result. The intercept of the regression was -0.1624 mV, which corresponds to an equivalent magnetic field of approximately -168 µT. This value is provided solely as a reference derived from the regression result rather than as a direct measurement, and a rigorous offset characterization using a higher-resolution measurement setup is therefore left for future work. In addition, the linearity characteristics discussed in this study remain unaffected by the absolute gain of the utilized amplifier, as the amplifier bias condition was fixed and the gain remained constant during the measurements. Since the main focus of this work is to demonstrate the validity of the proposed device structure in enabling appropriate current flow for in-plane magnetic field sensing, precise calibration of the amplifier gain and detailed offset characterization are left for future work.

By dividing the measured sensitivity by the estimated amplifier gain (10–30×), the intrinsic sensitivity of the Hall device element was estimated to be approximately 30–100 mV/T. Under the applied bias conditions of 1.6 V and 24 mA, the corresponding current-related sensitivity and voltage-related sensitivity, which were calculated as S/I_{bias} and S/V_{bias}, were estimated to be 1.3–4.2 V/T/A and 19–63 mV/T/V, respectively. While the voltage-related sensitivity falls within a reasonable range for silicon-based Hall elements as reported in [38], the current-related sensitivity appears relatively low when compared to the typical range of 100–1000 V/A/T for silicon-based Hall devices reported in [16]. This discrepancy suggests that not all of the supplied current contributes to Hall voltage generation. We attribute this behavior to the emitter-ring configuration adopted in this work, in which part of the bias current flows through regions that are not directly involved in the Hall sensing mechanism. On the other hand, this result implies that there remains headroom for further performance enhancement. We expect that optimizing the device geometry and current paths will enable more efficient current utilization and potentially lead to substantially higher intrinsic sensitivity.

In addition to this current distribution effect, the proposed VHD inherently includes a PN junction between the Deep N Well and the P Well along the current path. Because the

bias current must overcome the built in potential of this junction, the applied bias voltage needs to be higher than in conventional Hall devices formed entirely within a single carrier type region. This requirement reduces the achievable voltage related sensitivity. Moreover, the product of the bias current and the junction potential is dissipated as heat rather than contributing to Hall voltage generation, which increases power consumption and may elevate thermal noise during long term operation. Reducing these effects through improved junction design and biasing strategies is an important direction for future work.

From the measurement data shown in Fig. 12, a small variation is observed at each measurement point, which we used to estimate the magnetic field resolution of the proposed device. The magnetic resolution, B_{res}, was defined as

$$B_{\mathrm{res}} = \frac{V_{\mathrm{noise}}}{S}, \tag{3}$$

where V_{noise} represents the fluctuation amplitude of the output voltage and S denotes the magnetic sensitivity. As seen in Fig. 12, the magnitude of the output fluctuation tends to increase with the output voltage. Considering this dependence, the calculated resolution ranged from 1.03 mT to 6.72 mT. These values are higher than those of state-of-the-art Hall sensors reported in the literature, which is mainly attributed to the low-frequency noise components of the measurement setup and the absence of dedicated filtering or shielding in the present evaluation.

While these results quantify the resolution of the raw DC output, they do not represent the fundamental limit of the proposed device. The temporal characteristics of the measured noise indicate a slow low-frequency drift, which is consistent with flicker ($1/f$) noise typically observed in CMOS Hall structures operated in the near-DC regime. In HHDs, such low-frequency noise is effectively suppressed using current-spinning techniques as described in Section III-B. However, the proposed device includes a PN junction between the DNW and P-well, which restricts the current flow direction and prevents direct application of conventional current-spinning schemes. As an alternative approach, the Hall signal could be modulated by superimposing an AC component on the DC bias and employing synchronous detection. By translating the Hall voltage to a higher frequency band, this method can avoid the flicker-noise-dominated region and potentially improve the effective magnetic resolution. It should be noted, however, that introducing an AC modulation increases the instantaneous device current and may therefore elevate the shot-noise contribution. Thus, modulation-based readout techniques involve a trade-off between flicker-noise suppression and the increase in current-driven noise components, and exploring this balance represents an important direction for future work.

D. Evaluation of horizontal Hall sensor

This section evaluates the performance of the proposed HHD, which is designed to detect magnetic fields along the Z axis. A supply voltage of 2.01 V was applied to the sensor, resulting in a drive current of 40 mA. The magnetic flux density at the sensor position was swept from -73.4 mT to

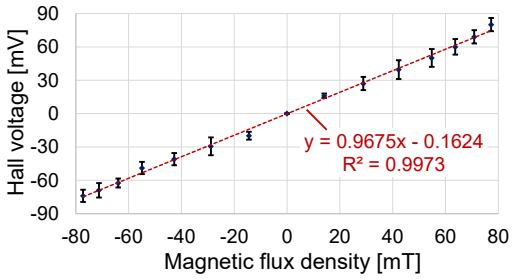

Fig. 12. Measured relationship between magnetic flux density and output voltage of the proposed VHD. Error bars represent the standard deviation across repeated measurements.

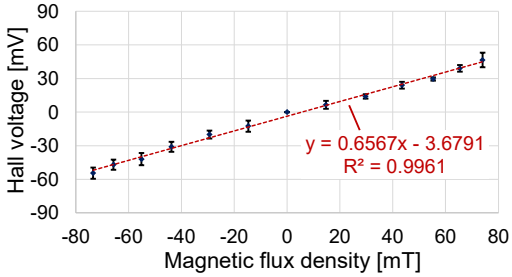

Fig. 13. Measured relationship between magnetic flux density and output voltage of the prototyped HHD. Error bars represent the standard deviation across repeated measurements

74.0 mT. The residual offset after four-phase current-spinning remained within the 0–1 mV noise floor of the measurement setup, indicating that any remaining offset was below the measurable limit. Fig. 13 presents the measurement result. As shown in Fig. 13, the output voltage of the HHD also varied linearly with the applied magnetic field, achieving a sensitivity of 656.7 mV/T. The linearity of the response was confirmed by a coefficient of determination of $R^2 = 0.996$.

E. Evaluation of angular response and cross-sensitivity

This section evaluates the angular stability and cross sensitivity of the proposed sensor structure under magnetic field directions that are not necessarily aligned with the primary coordinate axes. Cross-sensitivity refers to the undesired response of a magnetic sensor to magnetic field components along non-target axes. Ideally, each sensing axis in a three-axis sensor should respond exclusively to the magnetic field component along its designated direction and exhibit negligible sensitivity to orthogonal components. However, in practical implementations, particularly in VHDs for X and Y-axis sensing, non-negligible responses to orthogonal field components often arise due to structural asymmetries. As described in Section III-A, the proposed sensor employs an emitter-ring structure to suppress such effects and improve directional selectivity. This section experimentally validates its effectiveness in reducing cross-sensitivity.

To evaluate angular response, we fixed PCB with the mounted sensor onto a custom polyoxymethylene (POM) jig, allowing rotation around the X, Y, and Z axes, corresponding to roll, pitch, and yaw, respectively. Fig. 14 defines the rotation along each axis. By rotating the sensor in each direction while applying a constant magnetic field, we observe the variation

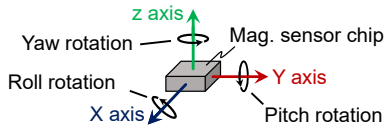

Fig. 14. Definition of each rotation.

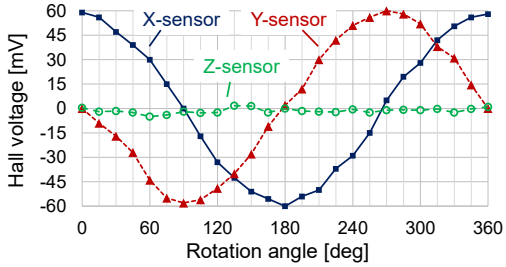

Fig. 15. Yaw angle rotation result.

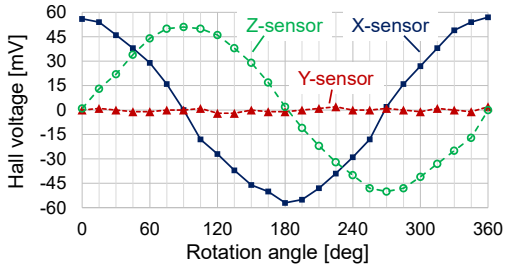

Fig. 16. Pitch angle rotation result.

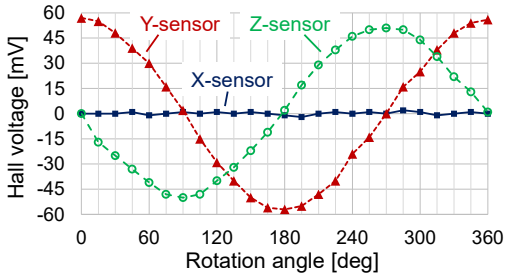

Fig. 17. Roll angle rotation result.

in each axis output and evaluate the degree of signal coupling among the axes.

Fig. 15 shows the results under yaw rotation. A constant magnetic field of 44.4 mT was applied along the positive X-axis. As the sensor rotated, the X- and Y-axis sensors exhibited cosine- and sine-like responses, respectively, due to their in-plane sensitivity. The Z-axis sensor output remained near zero, indicating proper axis orthogonality in the XY plane.

Fig. 16 presents the results under pitch rotation, with the magnetic field fixed at 44.4 mT along the positive X-axis. The Y-axis sensor output remained nearly constant, while the X- and Z-axis sensors showed cosine- and sine-like responses.

Fig. 17 shows the outputs under roll rotation, with the magnetic field applied along the positive Y-axis at 44.4 mT. The X-axis output stayed near zero, whereas the Y- and Z-axis sensors exhibited cosine- and sine-like variations, respectively. These results validate the proposed triaxial sensor's directional selectivity and effective decoupling among axes.

To quantify cross sensitivity, we adopt the normalized cross-sensitivity (CS) [29], [39], which compares the sensitivity of the orthogonal axis with the average of the two axes lying in the plane of rotation. It is defined as:

$$\mathrm{CS} = \frac{1}{2}\left(\frac{S_{\mathrm{cross}}}{S_{\mathrm{main1}}} + \frac{S_{\mathrm{cross}}}{S_{\mathrm{main2}}}\right) \times 100\%, \tag{4}$$

where S_{main1} and S_{main2} denote the sensitivities of the two main axes in the rotation plane, and S_{cross} is the sensitivity of the orthogonal axis. Each sensitivity S is calculated as the slope of the linear fit between the sensor output voltage and the magnetic field component. In the angular sweep measurements, multiple samples were acquired at each rotation angle and averaged to obtain a representative output voltage for that angle. Each sensitivity S is then extracted as the slope of the least-squares linear fit between these averaged voltages and the corresponding magnetic field component. Since CS is defined using the fitted slopes, constant output offsets primarily contribute to the intercept of the fit and do not affect the slope-based CS value, while random fluctuations of output are mitigated by the averaging and the subsequent fitting, as reflected by the resulting R^2 values.

During yaw rotation, only the X- and Y-axis Hall sensors exhibited sine- or cosine- like outputs, while the Z-axis sensor was expected to show minimal response, as shown in Fig. 15. The Z-axis output exhibited a sensitivity of approximately 0.01 mV/T with an R^2 value near zero, indicating negligible correlation with the in-plane field. In contrast, the X- and Y-sensors demonstrated high linearity, with R^2 values of 0.997 and 0.991, respectively. Based on these results, the normalized cross-sensitivity of the Z-axis was calculated to be 7.78×10^{-5}. Similarly, during pitch rotation, the Y-axis sensor showed minimal response, with a fitted sensitivity of approximately 0.01 mV/T and an R^2 value near zero. The normalized cross-sensitivity of the Y-axis was 8.09×10^{-5}. During roll rotation, the X-axis sensor output remained close to zero, with a fitted sensitivity of approximately 0.01 mV/T and R^2 near zero. The normalized cross-sensitivity of the X-axis was 8.03×10^{-5}. These results confirm that all axes exhibit extremely low cross-sensitivity, validating the effectiveness of the emitter-ring-based structure in achieving strong axis decoupling.

F. Comparison with related work

Table I summarizes the sensitivity and cross sensitivity of recent magnetic sensors and their fabrication processes. Compared to existing studies, the proposed sensor achieves a higher sensitivity, aided by on-chip amplifiers. While amplification typically increases the risk of cross-axis interference, the cross-sensitivity of the proposed sensor remains well below 0.01 % in all rotation modes, significantly outperforming the 1-6 % range reported in the literature. These results highlight the effectiveness of the proposed Hall device with symmetrical design, which suppresses interference between axes.

Importantly, the proposed VHD achieves this performance without relying on space-consuming STI structures or exclusively on the vertical Hall effect, which is highly sensitive to device geometry. These characteristics make the proposed structure well-suited for integration into compact sensor designs. To enable a fair comparison with prior work, we

TABLE I

SUMMARY OF MAGNETIC SENSORS SENSITIVITY AND CROSS-SENSITIVITY

Paper Source	Process	Sensitivity (mV/T)			Cross-Sensitivity (%)			Amplifier
		X-axis	Y-axis	Z-axis	X-axis	Y-axis	Z-axis	(used or not)
IEEE Sensors J., 2017 [40]	MEMS	77.5	78.6	77.4	3	3	3	-
MDPI Sensors., 2017 [41]	CMOS 180 nm	182	180	27.8	6	6	6	Yes
MDPI Sensors, 2021 [42]	CMOS 180 nm	534	525	119	4.8	4.7	2.9	-
Micromachines., 2023 [43]	CMOS 180 nm	485	484	237	3	3	3	-
IEEE Sensors J., 2024 [39]	CMOS 180 nm	148	147	19.2	1	1	1	No
IEEE Sensors J., 2025 [29]	CMOS-MEMS	560	556	-	2.6	2.5	-	-
Microsystems & Nanoeng., 2025 [44]	CMOS-MEMS	22.4	22.4	28.0	0.55	0.91	0.87	No
This work (evaluated in SectionIV-C&IV-D)	CMOS 180 nm	967.5	967.5	656.7	<0.01	<0.01	<0.01	Yes
This work (75 × 50 µm, X-axis sensor)	CMOS 180 nm	184.2	-	-	<0.01	-	-	Yes

also fabricated a scaled-down version of the sensor, with the smallest X-axis Hall element measuring 75 µm × 50 µm. This footprint is 41 % smaller in area than the 80 µm × 80 µm sensor reported in [41], with both designs employing on-chip amplification.

For clarity, we additionally compare the sensitivity normalized by device area, which enables a direct size-based comparison with STI-based structures. Notably, the sensor in [41] utilizes STI structures to enhance vertical sensitivity. The proposed device achieves a higher normalized sensitivity of 49.1 µV/T/µm^2, surpassing the 28.4 µV/T/µm^2 in [41] by approximately 72.89 %. This result highlights the efficacy of the proposed structure in achieving high sensitivity while enabling compact sensor integration.

V. CONCLUSION

This work presented a triaxial Hall sensor fabricated using a standard 180 nm CMOS process. The proposed structure leveraged the high conductivity of the DNW to enhance both horizontal and vertical current components, leading to improved Hall voltage generation. The sensor achieves sensitivities of 967.5 mV/T and 656.7 mV/T for vertical and horizontal Hall elements, respectively, with cross sensitivity well below 0.01 %. The proposed VHD avoids space-consuming STI structures and does not rely solely on the size-dependent horizontal Hall effect, making it suitable for compact, CMOS-compatible magnetic sensing applications.

REFERENCES

[1] C. Treutler, "Magnetic sensors for automotive applications," *Sensors and Actuators A: Physical*, vol. 91, no. 1-2, pp. 2–6, 2001.

[2] T. Reininger and C. Hanisch, "Magnetic field sensors for the industrial automation," *Sensors and Actuators A: Physical*, vol. 59, no. 1-3, pp. 177–182, 1997.

[3] L. Sarti, A. Sisto, L. Pilato, L. Di Piro, and L. Fanucci, "Platform based design of 3d hall sensor conditioning electronics," in *2015 11th Conference on Ph.D. Research in Microelectronics and Electronics (PRIME)*, 2015, pp. 200–203.

[4] C. Treutler, "Magnetic sensors for automotive applications," *Sensors and Actuators A: Physical*, vol. 91, no. 1, pp. 2–6, 2001, third European Conference on Magnetic Sensors & Actuators.

[5] M. Li, V. T. Rouf, M. J. Thompson, and D. A. Horsley, "Three-axis lorentz-force magnetic sensor for electronic compass applications," *Journal of Microelectromechanical Systems*, vol. 21, no. 4, pp. 1002–1010, 2012.

[6] M. Crescentini, S. F. Syeda, and G. P. Gibiino, "Hall-effect current sensors: Principles of operation and implementation techniques," *IEEE Sensors Journal*, vol. 22, no. 11, pp. 10 137–10 151, 2022.

[7] H. Heidari, E. Bonizzoni, U. Gatti, and F. Maloberti, "A cmos current-mode magnetic hall sensor with integrated front-end," *IEEE Transactions on Circuits and Systems I: Regular Papers*, vol. 62, no. 5, pp. 1270–1278, 2015.

[8] D. Murzin, D. J. Mapps, K. Levada, V. Belyaev, A. Omelyanchik, L. Panina, and V. Rodionova, "Ultrasensitive magnetic field sensors for biomedical applications," *Sensors*, vol. 20, no. 6, 2020.

[9] G. Rivero, M. Multigner, and J. Spottorno, "Magnetic sensors for biomedical applications," in *Magnetic Sensors*, K. Kuang, Ed. Rijeka: IntechOpen, 2012, ch. 7.

[10] R. Weiss, R. Mattheis, and G. Reiss, "Advanced giant magnetoresistance technology for measurement applications," *Measurement Science and Technology*, vol. 24, no. 8, p. 082001, jul 2013.

[11] P. Ripka, "Review of fluxgate sensors," *Sensors and Actuators A: Physical*, vol. 33, no. 3, pp. 129–141, 1992.

[12] E. S. Oliveros Mata, G. S. Cañón Bermúdez, M. Ha, T. Kosub, Y. Zabila, J. Fassbender, and D. Makarov, "Printable anisotropic magnetoresistance sensors for highly compliant electronics," *Applied physics. A, Materials science & processing*, vol. 127, no. 4, 2021.

[13] J. G. Deak, Z. Zhou, and W. Shen, "Tunneling magnetoresistance sensor with pt level 1/f magnetic noise," *AIP Advances*, vol. 7, no. 5, p. 056676, 03 2017.

[14] X. Yang, X. Zhao, Y. Bai, M. Lv, and D. Wen, "Two-dimensional magnetic field sensor based on silicon magnetic sensitive transistors with differential structure," *Micromachines*, vol. 8, no. 4, p. 95, 2017.

[15] C.-L. Dai, Z.-L. Zhu, C.-Y. Chang, and C.-C. Hsu, "Manufacturing and characterization of cmos-mems magnetic field microsensors with isolated cavities," *Journal of Micromechanics and Microengineering*, vol. 34, no. 4, p. 045004, mar 2024.

[16] M. A. Khan, J. Sun, B. Li, A. Przybysz, and J. Kosel, "Magnetic sensors-a review and recent technologies," *Engineering Research Express*, vol. 3, no. 2, p. 022005, 2021.

[17] K. Veselinov, "A 3-d hall sensor for precise angular position measurements," *Turk J Phys c UB ˙ ITAK*, vol. 31, pp. 97–101, 01 2007.

[18] C. Wouters, V. Vranković, C. Rössler, S. Sidorov, K. Ensslin, W. Wegscheider, and C. Hierold, "Design and fabrication of an innovative three-axis hall sensor," *Sensors and Actuators A: Physical*, vol. 237, pp. 62–71, 2016.

[19] C. Schott, R. Racz, and S. Huber, "Cmos three axis hall sensor and joystick application," in *SENSORS, 2004 IEEE*, 2004, pp. 977–980 vol.2.

[20] D. R. Popovic, S. Dimitrijevic, M. Blagojevic, P. Kejik, E. Schurig, and R. S. Popovic, "Three-axis teslameter with integrated hall probe," *IEEE Transactions on Instrumentation and Measurement*, vol. 56, no. 4, pp. 1396–1402, 2007.

[21] H. Fan, S. Li, V. Nabaei, Q. Feng, and H. Heidari, "Modeling of three-axis hall effect sensors based on integrated magnetic concentrator," *IEEE Sensors Journal*, vol. 20, no. 17, pp. 9919–9927, 2020.

[22] M. Paranjape, I. Filanovsky, and L. Ristic, "A 3-d vertical hall magnetic-field sensor in cmos technology," *Sensors and Actuators A: Physical*, vol. 34, no. 1, pp. 9–14, 1992.

[23] K. Maenaka, H. Fujiwara, T. Ohsakama, M. Ishida, T. Nakamura, A. Yoshida, and Y. Yasuda, "Integrated magnetic vector sensor," in *Proc. of the 5th Sensor Symposium*, 1985, pp. 179–183.

[24] V. Zieren and B. P. Duyndam, "Magnetic-field-sensitive multicollector npn transistors," *IEEE Transactions on Electron Devices*, vol. 29, no. 1, pp. 83–90, 1982.

[25] S. Kordic and P. J. Munter, "Three-dimensional magnetic-field sensors," *IEEE Transactions on Electron Devices*, vol. 35, no. 6, pp. 771–779, 1988.

[26] C. S. Roumenin, "Bipolar magnetotransistor sensors. an invited review," *Sensors and Actuators A: Physical*, vol. 24, no. 2, pp. 83–105, 1990.
[27] R. Besserer, Y. Mermoud, T. Gnos, S. Reymond, P. Kejik, J. Muttersbach, C. Würsch, and S. Huber, "Non-orthogonality and amplitude mismatch of vertical hall based angular sensors due to in-plane shear stress," in *IEEE Sensors*, 2022, pp. 507–510.
[28] S. V. Lozanova, M. L. Ralchev, A. J. Ivanov, and C. S. Roumenin, "Three-contact in-plane sensitive hall devices," in *2022 XXXI International Scientific Conference Electronics (ET)*, 2022, pp. 180–185.
[29] Z.-X. Dai, R.-W. Tsai, and Q.-H. Shih, "High-sensitivity magnetic field sensors manufactured utilizing cmos-mems technology," *IEEE Sensors Journal*, vol. 25, no. 6, pp. 9540–9549, 2025.
[30] R. Popovic, P. Drljaca, C. Schott, and R. Racz, "A new cmos hall angular position sensor (neuer cmos-hall-winkelpositionssensor)," *tm - Technisches Messen*, vol. 68, no. 6, p. 286, 2001.
[31] C. Schott, R. Racz, and S. Huber, "Smart cmos sensors with integrated magnetic concentrators," in *IEEE SENSORS*, 2005, pp. 959–962.
[32] X. Li, X. Zhao, and D. Wen, "Characteristics of a magnetic field sensor with a concentrating-conducting magnetic flux structure," *Sensors*, vol. 19, no. 20, 2019.
[33] R. Popovic, "The vertical hall-effect device," *IEEE Electron Device Letters*, vol. 5, no. 9, pp. 357–358, 1984.
[34] P. C. De Jong, F. R. Riedijk, and J. van der Meer, "Smart silicon sensors-examples of hall-effect sensors," in *SENSORS, 2002 IEEE*, vol. 2. IEEE, 2002, pp. 1440–1444.
[35] E.-H. Toh, Y. Sun, P. Zheng, M. Shajan, P. Cao, M. N. Islam, J.-Y. Wong, P. Arikath, R. Jain, T. L. Tan, and E. Quek, "A modular three-dimensional hall effect sensor for performance optimization," *IEEE Sensors Journal*, vol. 22, no. 12, pp. 11 256–11 263, 2022.
[36] V. Mosser, N. Matringe, and Y. Haddab, "A spinning current circuit for hall measurements down to the nanotesla range," *IEEE Transactions on Instrumentation and Measurement*, vol. 66, no. 4, pp. 637–650, 2017.
[37] C. Hu, *Modern Semiconductor Devices for Integrated Circuits*. Prentice Hall, 2010. [Online]. Available: https://books.google.co.jp/books?id=PosRbWdafnsC
[38] J. Lenz and S. Edelstein, "Magnetic sensors and their applications," *IEEE Sensors journal*, vol. 6, no. 3, pp. 631–649, 2006.
[39] Z.-X. Dai and M.-H. You, "Modeling and measurement of cmos-based three-axis magnetic field sensors with low cross-sensitivity," *IEEE Sensors Journal*, vol. 24, no. 21, pp. 34 217–34 227, 2024.
[40] X. Zhao, Y. Bai, Q. Deng, C. Ai, X. Yang, and D. Wen, "Research of the monolithic integrated 3-d magnetic field sensor based on mems technology," *IEEE Sensors Journal*, vol. 17, no. 18, pp. 5849–5856, 2017.
[41] W.-R. Chen, Y.-C. Tsai, P.-J. Shih, C.-C. Hsu, and C.-L. Dai, "Magnetic micro sensors with two magnetic field effect transistors fabricated using the commercial complementary metal oxide semiconductor process," *Sensors*, vol. 20, no. 17, p. 4731, 2020.
[42] C.-H. Wu, P.-J. Shih, Y.-C. Tsai, and C.-L. Dai, "Manufacturing and characterization of three-axis magnetic sensors using the standard 180 nm cmos technology," *Sensors*, vol. 21, no. 21, p. 6953, 2021.
[43] C.-H. Wu, C.-C. Hsu, Y.-C. Tsai, C.-Y. Lee, and C.-L. Dai, "Design and measurement of microelectromechanical three-axis magnetic field sensors based on the cmos technique," *Micromachines*, vol. 14, no. 5, p. 1038, 2023.
[44] J. Ruggeri, U. Ausserlechner, H. Köck, and K. M. Dowling, "Inverted pyramid 3-axis silicon hall-effect magnetic sensor with offset cancellation," *Microsystems & Nanoengineering*, vol. 11, no. 1, p. 26, 2025.

Yuhao Wang received the B.E. degree from the School of Computer and Electronic Information /School of Artificial Intelligence, Nanjing Normal University, Nanjing, China, in 2023, and the Master of Informatics degree from the Graduate School of Informatics, Kyoto University, Kyoto, Japan, in 2025. He is currently an Analog Engineer with Renesas Electronics Corporation, Japan. His current work focuses on analog design for automotive power management integrated circuits (PMICs). His research interests include inductive magnetic sensors, CMOS devices, and automotive power electronics.

Toshihisa Tanaka received the B.E. degree in Engineering in 2022 and the M.S. degree in Informatics in 2024, both from Kyoto University, Japan, where He is currently pursuing his Ph.D. degree. His research interests include CMOS magnetic field sensors and magnetic field based indoor localization.

Tomochika Harada received the B.E. degree in Information Engineering from Tohoku University in 1995, and M.E. and Ph.D. degrees in Information Science from the Graduate School of Information Sciences at Tohoku University in 1997 and 2000, respectively. From 2000 to 2003, he joined Chuo University as a technical staff member. Since 2003, he has been an Assistant Professor at Yamagata University. His current research interests include ultra-low-power mixed-signal circuits, MOSFET-based semiconductor smart sensors, and ICT/IoT systems for visualizing various aspects of life. He is a member of the Institute of Electrical Engineers in Japan (IEEJ), the Institute of Electronics, Information and Communication Engineers (IEICE), the Japan Society of Applied Physics (JSAP), and the IEEE.

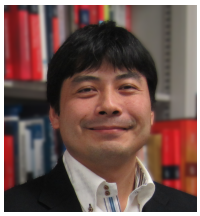

Masanori Hashimoto (Senior Member, IEEE) received the B.E., M.E., and Ph.D. degrees in communications and computer engineering from Kyoto University, Kyoto, Japan, in 1997, 1999, and 2001, respectively. He is currently a Professor with the Graduate School of Informatics, Kyoto University. His research interests include VLSI design for reliability, timing and power integrity analysis, reconfigurable computing, soft error characterization, and low-power circuit design. He was the TPC chair for Asia and South Pacific Design Automation Conference (ASP-DAC) 2022 and International Midwest Symposium on Circuits and Systems (MWSCAS) 2022. He was/is on the Technical Program Committees of international conferences, including Design Automation Conference (DAC), International Conference on Computer-Aided Design (ICCAD), International Test Conference (ITC), Symposium on VLSI Circuits, and Design, Automation and Test in Europe Conference (DATE). He served as the Editor-in-Chief for *Microelectronics Reliability* (Elsevier) and an Associate Editor for IEEE TRANSACTIONS ON VERY LARGE SCALE INTEGRATION (VLSI) SYSTEMS, IEEE TRANSACTIONS ON CIRCUITS AND SYSTEMS—I: REGULAR PAPERS, and *ACM Transactions on Design Automation of Electronic Systems* (TODAES).

Ryo Shirai (S'16–M'21) received the B.E., M.E., and Ph.D. degree in information systems engineering from Osaka University, Suita, Japan, in 2016, 2018, and 2021 respectively. He is currently an Assistant Professor with the Department of Communication and Computer Engineering, Graduate School of Informatics, Kyoto University, Kyoto, Japan. His current research interests include analog circuit design, embedded systems, and sensor systems. Dr. Shirai is a member of the Institute of Electronics, Information and Communication Engineers (IEICE).